Civil Engineering Infrastructures Journal xx,xx
DOI: 10.22059/ceij.2026.405755.2430

# Post-Fire Performance of Steel-Fiber, MIBA-Blended Concrete Enhanced by Inorganic Self-Healing

**Dost Rehman[1], Muhammad Noman[1*], Muhammad Muneeb Nawaz[1], Nisar Ali Khan[1], Tufail Mabood[2]**

1. Department of Civil Engineering, Faculty of Engineering & Technology, International Islamic University Islamabad (IIUI), Pakistan.
2. Department of Civil Engineering, University of Engineering & Technology (UET), Pakistan.

Corresponding Author Email: muhammad.noman@iiu.edu.pk

ORCID: Muhammad Noman [0000-0001-9054-3508],

Accepted / Not Edited

Received: 07/11/2025
Revised: 20/05/2026
Accepted: 05/08/2026

## Abstract

This study examines the post-fire performance and inorganic self-healing of concretes incorporating municipal solid-waste incineration bottom ash (MIBA) and steel fibers. The combined effects of MIBA dosage and fibers used with inorganic healing granules on damage and recovery after heating are insufficiently resolved. The objective was to quantify how MIBA (0, 5, 10, 15% cement replacement) and steel fibers (0, 0.5, 1.0%) influence compressive strength and ultrasonic pulse velocity (UPV) at ambient, after 400 °C exposure, and after re-curing, and to

identify workable MIBA levels and fiber benefits. A 4×3 factorial experimental program consists of casting concrete cubes with 2% (by mass of concrete) epoxy-coated inorganic healing granules. The samples were tested in three states, control, heated, and 28-day water re-cured. Increasing MIBA lowered baseline strength (15%) and reduced residual and healed ratios, with the sharpest penalties at 15%. Fibers had limited effect on peak ambient strength but improved post-fire recovery, raising residual ratios and healed ratios, with the largest proportional gains at higher MIBA. Overall, up to 10% MIBA offers manageable trade-offs, while pairing fibers with inorganic granules enables robust post-fire strength and stiffness recovery after heat exposure.

**Keywords:** MIBA; Steel Fibers; Self-healing; Fire Exposure; Municipal Waste; Elevated Temperature; Recuring

# 1 Introduction

The high carbon content of concrete is still a major problem for the long-term sustainability of the built environment. The process and energy emissions from making clinker account for about 7–8% of all anthropogenic $CO_2$, making cement one of the biggest single industry sources of greenhouse gases (Massoumi Nejad et al., 2025; Volaity et al., 2025). In parallel, municipal solid waste incineration produces substantial volumes of bottom ash that are often stockpiled or dumped in landfilled even though they are of value as secondary resources for construction materials. Recent reviews point to municipal solid waste incineration bottom ash (MIBA) as a candidate for partial substitution in cementitious systems, with potential to reduce clinker intensity and divert waste streams when appropriately processed (Magnuson et al., 2023; Nawaz et al., 2025).

Municipal solid-waste incineration bottom ash (MIBA) is the mineral-rich residue discharged from grate furnaces after quenching/aging and typically contains glassy silicates, ceramics, and ferrous/non-ferrous metals. Its grading and chemistry vary markedly by plant, feedstock, and operating conditions, which motivates strict processing and quality control before any cementitious use (Lu et al., 2020). In order to stabilize surface chemistry and enhance environmental performance (e.g., decreased metal leaching), standard pre-treatments include mechanical separation followed by wet extraction to reduce soluble salts and aging or accelerated carbonation (Arickx et al., 2006; Astrup, 2007). The study of MIBA within cementitious matrices presents significant complexities. Previous studies indicate that treated MIBA can serve as a fine aggregate replacement and, when finely ground, as a supplementary cementitious material (SCM) in concrete and mortar (Bawab et al., 2021; Chang et al., 2006; Chen et al., 2023; Mafalda Matos & Sousa-Coutinho, 2022). Field and lab tests on cement and concrete also show that MIBA works well in terms of mechanical and durability performance when used in controlled quantities (Silva et al., 2019; Węgliński & Martysz, 2024).

Structural concretes must perform not only in service but also after accidental heating because thermal excursions can quickly reduce stiffness and compressive strength (Noman, Yaqub, Fahad, et al., 2022). Temperatures between 300 and 500 °C have the most important effects as they speed up the dehydration of cement hydrates, differential thermal strains, and microcracking that depress

Accepted / Not Edited

both stiffness and strength (Ma et al., 2015; Noman et al., 2024). The literature predict that strength will drop significantly by 400 °C, which is a common temperature used in many testing programs (Tufail et al., 2016). The post-heat curing can partially reverse these losses by promoting rehydration and crack infill, particularly under water immersion (Li et al., 2020; Noman, Yaqub, Abid, et al., 2022).

Steel fibers are incorporated chiefly to restrain crack opening and sustain post-cracking load transfer rather than to raise the peak compressive strength (ACI-544.4, 2018). In the 300–500 °C range heat exposures, steel fiber reinforced concrete (SFRC) typically shows higher residual compressive strength and toughness than plain concrete because fibers bridge and stabilize thermally induced microcracks (Lau & Anson, 2006; Modarres & Ghalehnovi, 2024). For self-healing processes, keeping crack widths sub-millimetric is critical to enable water access and reaction products to seal the damage. By limiting crack opening and maintaining connectivity, steel fibers enhance both autogenous and autonomous healing efficacy (De Belie et al., 2018).

Inorganic self-healing in cementitious systems relies on crack-triggered reactions that recreate or densify hydration products and seal transport paths without external intervention. Typical agents include alkali silicates (e.g., sodium/potassium silicate), crystalline admixtures based on reactive silicates/carbonates, and lime or MgO bearing phases. These are delivered as free powders, embedded in porous/ceramic carriers, or micro-encapsulated to ensure release when cracking or re-curing occurs (De Belie et al., 2018). When water enters, alkali silicates interact with portlandite to form C–S–H/C–A–S–H gels, whereas carbonate processes produce $CaCO_3$ infill, both of which decrease crack conductivity and restore stiffness and strength (De Belie et al., 2018; Qian et al., 2010). In the post-heating context, re-curing provides the moisture and ions that catalyze these inorganic reactions, so pairing a small dose of inorganic healing granules with crack-width control from steel fibers is mechanistically synergistic. Fibers keep cracks narrow/connected, and the healing agent promotes rehydration and mineral infill along the damaged network (Huang et al., 2014; Van Tittelboom & De Belie, 2013).

While MIBA, steel fibers and inorganic self-healing agents have all been studied in the context of cementitious systems, the current literature deals with them primarily separately and under different loading conditions. The studies conducted at MIBA have been mainly about ambient mechanical performance and durability, and have limited scope with regards to the post-fire condition. The current work on steel fibers in fire exposed concrete has mostly been conducted in plain or conventional SCM concrete, where the fibers are known to be effective in the stabilization of thermally induced microcracks and they are not associated with a subsequent healing phase. Studies of the inorganic self-healing, on the other hand, have usually been carried out on virgin or mechanically pre-cracked samples, and it is not yet well established whether these agents are effective after thermal degradation of matrix. Therefore, the overall behavior of a MIBA blended, steel-fiber-reinforced concrete loaded with an inorganic healing granulate has never been quantified in a single controlled program that has been run through a complete heat–damage–recovery cycle. The present study fills this void by reporting, for the same set of mixes, the initial,

Accepted / Not Edited

residual (after 400 °C) and recovered (after 28-day water re-curing) compressive strength and UPV, which helps to understand the relative contributions of MIBA dosage and fiber content and the practical utility of combining fibers with a water-activated inorganic healing agent to provide post-fire performance.

# 2 Materials and Methods

## 2.1 Materials

Ordinary Portland cement (OPC) was used in a nominal proportion of 1:1.5:3 (cement:fine aggregate:coarse aggregate) by weight with a fixed water-to-binder ratio (w/b) of 0.60. Locally available crushed limestone aggregates were used as the primary aggregate system due to their ready availability in the region and consistent quality control. Aggregates were used in saturated-surface-dry (SSD) condition and conformed to conventional grading and cleanliness requirements (ASTM-C33/C33M-18, 2018). Moisture corrections were applied prior to batching to maintain the target w/c ratio.

Municipal incinerated bottom ash (MIBA) was obtained from a local municipal solid-waste incineration plant. The ash was collected from the furnace bottom after the quench/de-ashing stage, air-dried, and screened to remove oversized particles and debris. Ferrous inclusions were removed magnetically, and any visible non-mineral contaminants were hand-picked where necessary. The ash was then oven-dried (105 °C) to constant mass and sieved to obtain a fine fraction (passing 75 μm) suitable for partial cement replacement. The retained coarse fraction was discarded. Figure 1 (a) shows the screened MIBA used in this study. XRD (see Figure 2) of the MIBA shows strong crystalline reflections, dominated by quartz (26.5°) and calcite (29.5°), with weaker peaks attributable to hematite and corundum. The predominance of crystalline phases indicates low intrinsic reactivity, suggesting that additional conditioning e.g., fine grinding, washing/aging, or accelerated carbonation may be required to improve its reactivity. The XRF results showing the percentage oxides of MIBA are compared with the OPC are provided in Table 1. MIBA replaced cement at 0, 5, 10, and 15% by mass of cement, with the total binder mass held constant across mixes. The ash was stored in sealed containers to prevent moisture uptake prior to use.

Commercial carbon-steel fibers were used with the nominal dimensions of 25 mm (length), and 0.5 mm (diameter). The mechanical properties of the fibers were taken as reported by the supplier i.e., Tensile strength = 345 MPa and elastic modulus = 200 GPa. The fibers were used as received and stored dry. Figure 1 (b) shows the steel fibers used in this study.

An inorganic, multi-component healing agent was produced as spherical granules and later coated to improve handling and resist agglomeration during mixing. The core powder blend comprised sodium silicate, sodium carbonate, sodium hydroxide, quicklime (CaO), and bentonite clay in the mass fractions shown in Table 2. Dry powders were blended to homogeneity, after which distilled water was introduced slowly in a rotary granulation mixer to nucleate and round the particles. The wet granules were tray-dried in a ventilated oven for 24 h, then allowed to cool to room temperature. A thin epoxy-resin coating was applied as a protective barrier; immediately after

Accepted / Not Edited

coating, the granules were lightly dusted with cement to suppress surface tack and reduce inter-particle adhesion. The resulting granules exhibited an average diameter of 8 mm (visual sieve check), a smooth outer shell, and sufficient handling robustness for batching. Figure 1 (c) shows prepared granules used in this study. Prior to use they were stored in sealed containers. In the concrete mixtures, the granules were dosed at 2% by mass of concrete.

The "8 mm granule" size was chosen as an acceptable compromise for several competing requirements. Smaller granules (less than about 4-5 mm) were hard to make regularly with the powder blend used in the Rotary Granulation Mixer and had higher attrition during the wet mixing, which reduced the integrity of the protective epoxy coating prior to placement. Granules of 8 mm, on the other hand, were strong enough to remain unaffected by the entire mixing process with the coating on, so as to avoid the sodium silicate and quicklime reacting with mixing water prematurely. The selected size is also in a relatively similar size range with the smaller sized coarse aggregate in the mixes (nominal maximum size 20 mm) and therefore the granules fall within the size range of the matrix that is already designed to accommodate them. With the 2% mass dosage used, the average number of granules per 100 $mm^3$ is in the order of 15 - 20, which allows for a fairly even distribution of healing agent. Visual examination of fractured control specimens did not show preferential clustering at the base of the moulds which indicated that the relatively high rounded granule shape, the cement dusting used after coating and the moderate mix viscosity were adequate to reduce segregation during placing.




*Figure 1: Principal constituents used in the study: (a) processed MIBA fines, (b) steel fibers, and (c) epoxy-coated inorganic self-healing granules*

Accepted / Not Edited

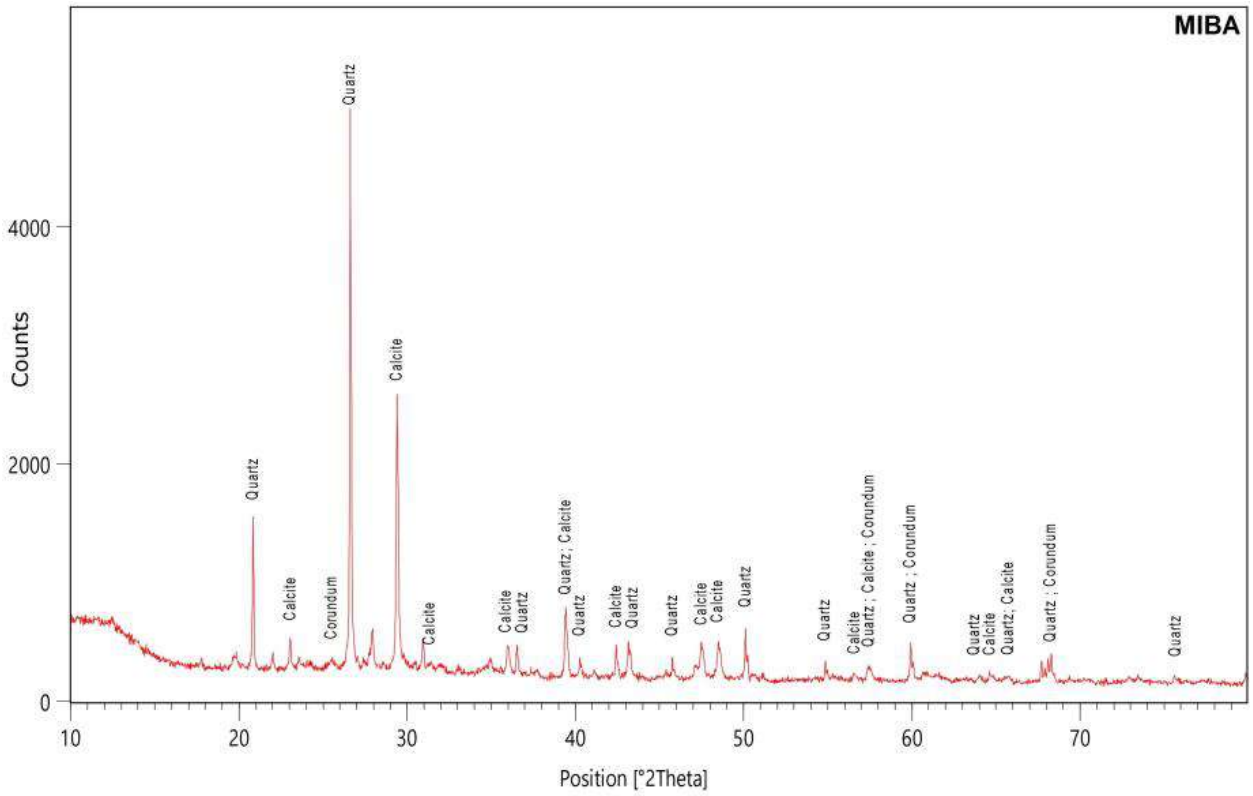



*Figure 2: X-ray Diffraction of MIBA*

*Table 1: Comparison (% Weight) of Oxides using XRF*

| Oxide | MIBA | OPC |
|---|---|---|
| CaO | 44.54 | 62.01 |
| $SiO_2$ | 21.86 | 21.01 |
| $Al_2O_3$ | 7.48 | 5.32 |
| $Fe_2O_3$ | 4.47 | 3.19 |
| $SO_3$ | 2.55 | 1.55 |
| MgO | 2.79 | 2.62 |
| $K_2O$ | 1.63 | - |
| $Na_2O$ | 1.98 | - |
| Others | 0.01 | - |
| LOI | 12.60 | 1.88 |

*Table 2: Composition of self-healing granule*

| Raw Material | Sodium Silicate | Sodium Carbonate | Sodium Hydroxide | Quick Lime (CaO) | Bentonite |
|---|---|---|---|---|---|
| % Composition | 40 | 20 | 10 | 20 | 10 |

Accepted / A

## 2.2 Specimen Preparation

All concretes were produced by mass in a laboratory pan mixer (0.15 $m^3$ nominal, 25 rpm) at (25 ± 2) °C. For each target combination of MIBA replacement (0, 5, 10, 15 % by mass of cement) and steel-fiber dosage (0, 0.5, 1.0%), the binder was pre-blended (OPC + MIBA) to the specified level and combined with saturated surface dry crushed limestone aggregates. Mixing followed a fixed sequence and timing to ensure repeatability. First the dry blending for 60 s of pre-blended binder and aggregates, after which water was added to achieve w/b = 0.60 followed by 120 s wet mixing. Steel Fibers were gradually added for over 60 s with a further 60 s mixing to obtain visual uniformity. Finally, the inorganic self-healing granules (average diameter = 8 mm) dosed at 2% by mass of concrete were added for 30 s. The slow addition of the epoxy-coated granules was to avoid abrasion while achieving even distribution.

Fresh properties were checked on every batch and used as acceptance criteria with slump (ASTM-C143, 2015) targeted 60–90 mm, and density (ASTM-C138, 2023) within ± 20 $kg \cdot m^{-3}$ of the control-mix mean. No chemical admixtures were used. Fibers were dosed as used in the experimental program and added slowly to avoid balling. Fresh concrete was placed into steel cube moulds of 100 mm internal dimension, cleaned and lightly oiled beforehand. Moulds were filled in two approximately equal lifts; each lift received 10–15 s of equivalent internal rodding to expel entrapped air. Surfaces were struck off flush and covered to limit evaporation. Demoulding occurred at 24 h, after which specimens were transferred to water curing at 20 °C until the designated reference age (28 d) prior to any further conditioning. Curing tanks were refreshed at least twice weekly.

The nomenclature of the samples is provided in the Table 3. As an example, $M_{15}$–$S_{10}$–F–$r_3$ would mean a specimen with 15 % MIBA replacement and 1% steel fiber dosage, heated to 400 °C, and the third sample of the same condition. The workflow for the experimentation is provided in Figure 3.

Accepted / Not Edited

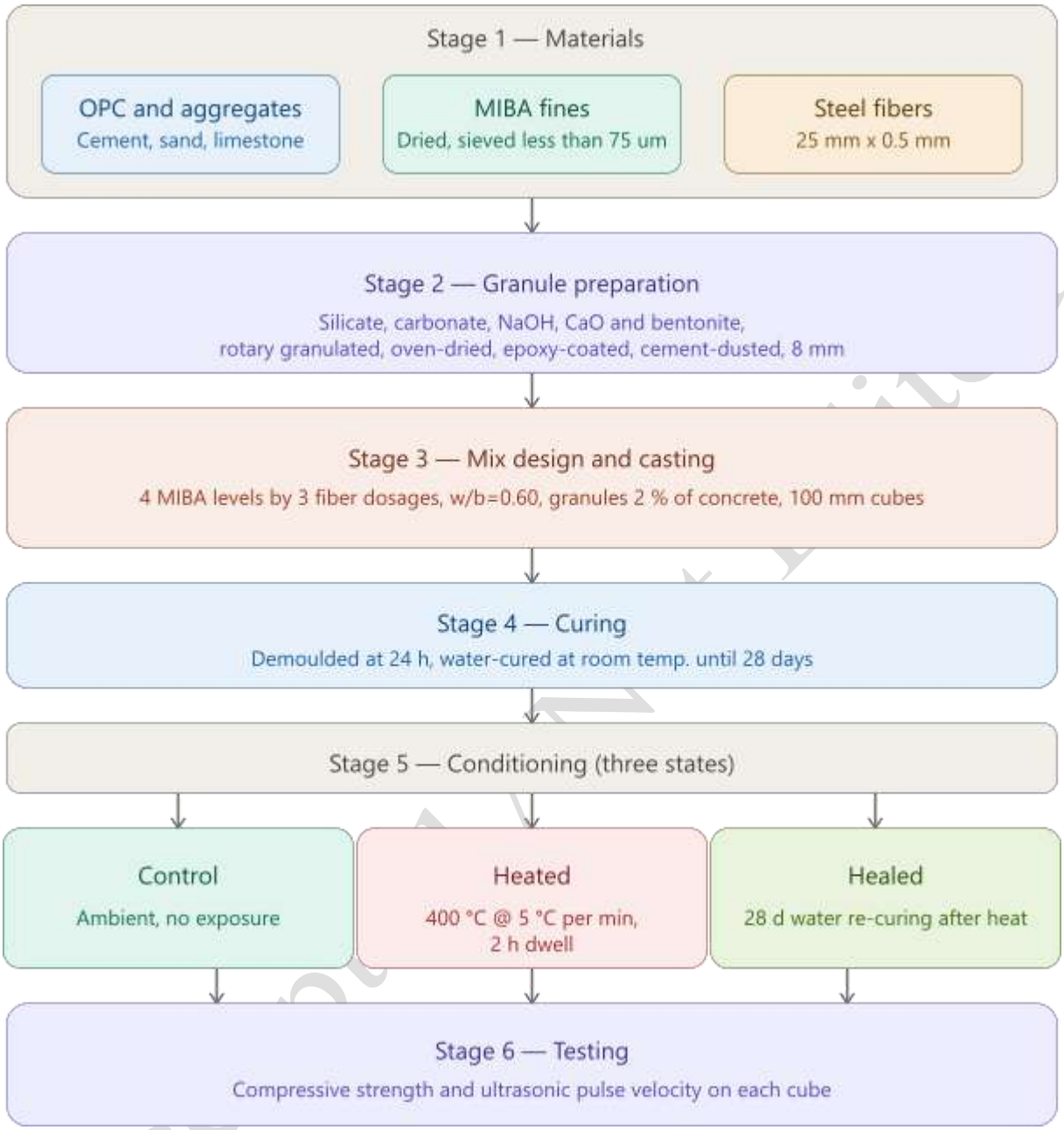



*Figure 3: Schematic overview of the experimental workflow from materials and granule preparation through casting, curing, conditioning (Control, 400 °C, Healed), and testing*

*Table 3: Specimen nomenclature and coding scheme*

| Code Field | Description | Allowed Values | Example |
|---|---|---|---|
| $M_{xx}$ | MIBA replacement (% of cement, rounded to 2 digits) | 00, 10, 20, 30 | $M_{20}$ → 20% MIBA |
| $S_{yy}$ | Steel-fiber dosage (%, expressed as used; 0.5 → 05) | 00, 05, 10 | $S_{05}$ → 0.5% steel fiber |

| | | | |
|---|---|---|---|
| H /C/R | Conditioning state | C = Control; F = Furnace 400 °C; R = Post-heating healed | F → furnace-exposed |
| $r_n$ | Replicate index | $r_1$, $r_2$, $r_3$ | $r_2$ → replicate 2 |

## 2.3 Heating, Curing & Testing

Before furnace exposure, all specimens allocated to the thermal set were air-dried for 72 h at 20–25 °C and 50–60% RH to harmonize moisture content and reduce spalling risk. Thermal exposure was carried out in a programmable furnace using a 5 °C·min$^{-1}$ ramp to 400 °C, 2 h peak dwell, and closed-door cooling to < 100 °C prior to handling. The time-temperature profile, measured using the built-in K-type thermocouple inside the furnace is provide as Figure 4.

Specimens in the post-heating repaired (healed) set were, after cooling, immersed in water at (20 ± 2) °C for 28 d (no external repair agents were applied). Healing duration was recorded from immersion start to the test day. Except for the specified conditioning (Control; 400 °C; Healed), production and curing procedures were identical across all mixes.

For each of the 12 mix combinations (4 × 3 factorial), three 100-mm cubes per condition (Control, 400 °C, Healed) were cast, yielding 108 cubes in total. Allocation to conditions was randomized immediately after demoulding to minimize batch effects. The above mixing sequence, timings, acceptance windows, and conditioning parameters are consistent with published practice for fiber-reinforced concretes and low-temperature fire exposures (400 °C) used to study residual and recovered performance.

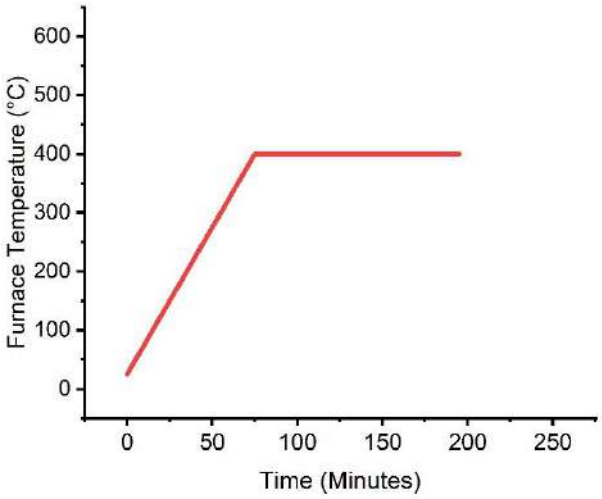



*Figure 4: Furnace time-temperature profile*

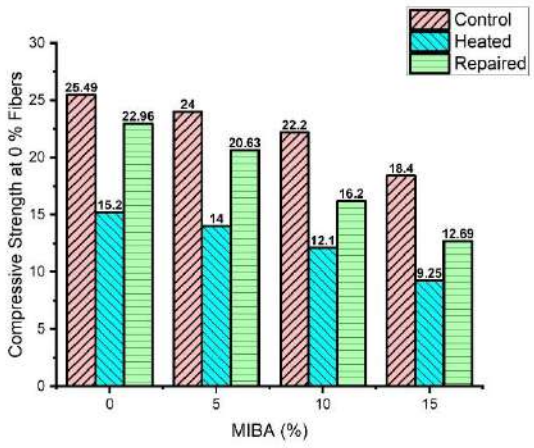
Accepted / Not Edited

# 3 Results and Discussions

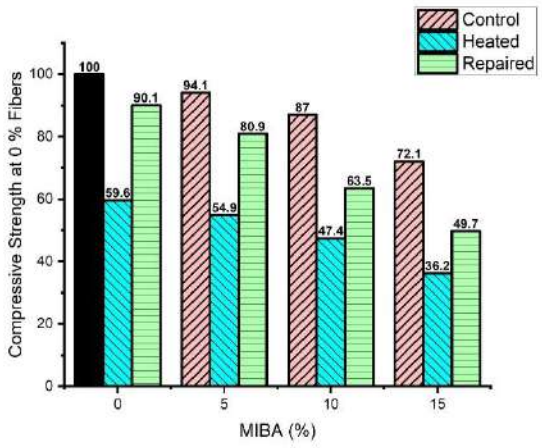
## 3.1 Effects of MIBA on Compressive Strength

Figure 5 shows that introducing municipal-solid-waste incineration bottom ash (MIBA) as a cement replacement produced a clear, dosage-dependent reduction in compressive strength. Averaged across fiber dosages, the control strength declined from 26.2 MPa at 0% MIBA to 24.6 MPa (5%), ≈22.7 MPa (10%), and 19.0 MPa (15%) (27% decrease over 0–15%). After heating to 400 °C, the retained capacity also fell progressively with MIBA. The 400 °C/Control ratio moved from 0.61 (0%) and 0.59 (5%) to 0.56 (10%), then 0.52 (15%). Following water recuring, recovery remained high at low MIBA and dropped more noticeably only at the upper level: Healed/Control 0.94 (0%), 0.89 (5%), 0.79 (10%), and 0.75 (15%).

It can be noted that across 0–10% MIBA, the additional penalty, both in thermal loss and in post-heating recovery, is modest. In this range, fine MIBA can act as an inert/filler and the dilution of clinker is limited, so the matrix retains much of its load-bearing capacity and remains responsive to re-hydration during water curing. Moreover, at 15% MIBA the effect becomes pronounced where, baseline strength drops more steeply, the residual capacity after 400 °C is lower, and the healing ratio diminishes. This transition is consistent with (i) clinker dilution (fewer hydration products available to carry load), (ii) higher capillary porosity and a weaker ITZ, which aggravate microcracking under heat, and (iii) reduced re-hydration potential because less unhydrated clinker remains to fuel strength recovery. In short, MIBA has only a small additional influence on strength loss and recovery up to about 10%, whereas 15% marks a clear deterioration in both residual strength and regain.




(a)




(b)

Not Edited

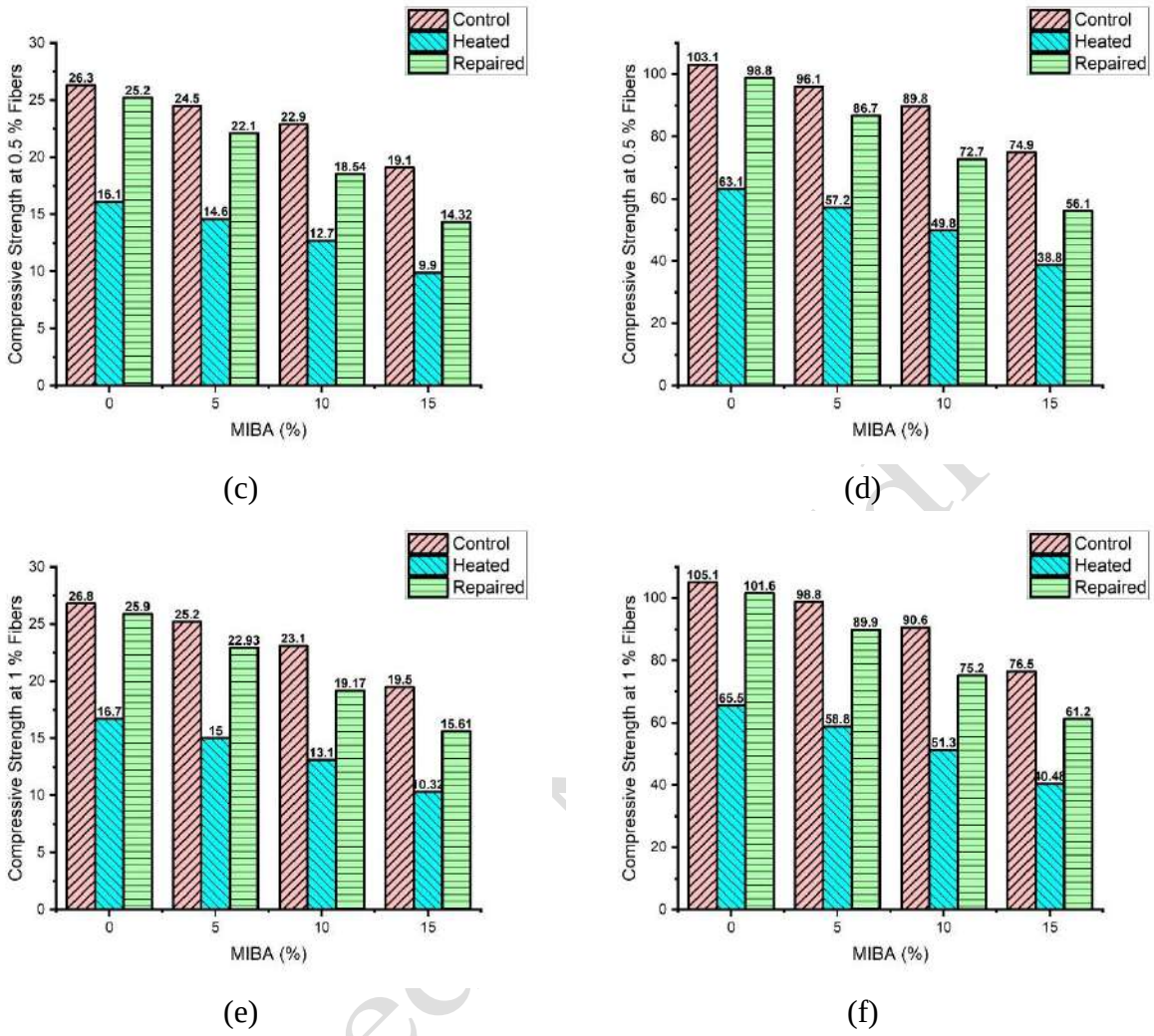



*Figure 5: Effects MIBA variation on Compressive Strength*

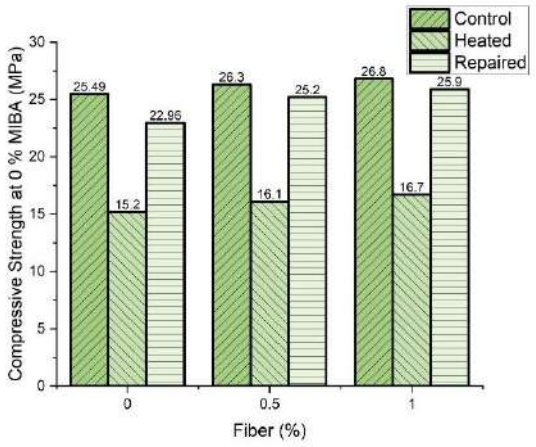
## 3.2 Effects of Steel Fibers on Compressive Strength

Figure 6 shows that at ambient conditions, steel fibers had little influence on peak compressive strength (only ±1 MPa changes at a given MIBA level), which aligns with the established view that fibers primarily enhance toughness, crack control, and post-peak behavior rather than the elastic peak. Their effect becomes consequential once the material is thermally damaged and subsequently healed.

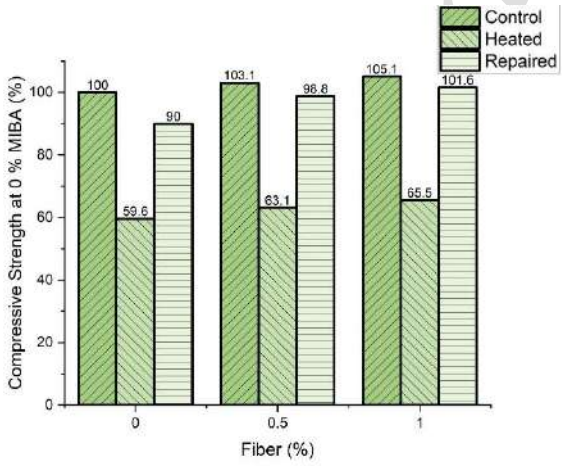
After exposure to 400 °C, fibers improved the retained capacity: the mean 400 °C/Control ratio increased from 0.557 (0% fibers) to 0.570 (0.5%) and 0.578 (1.0%), i.e., a 2 to 4 percentage-point gain. This improvement is attributable to crack-bridging and stress redistribution across fiber–matrix interfaces, which limits crack opening and reduces the effective loss of load-bearing area (and the risk of local spalling). After water recuring, the fiber benefit strengthened further: Healed/Control rose from 0.795 (0% fibers) to 0.855 (0.5%) and 0.877 (1.0%), reflecting 6 to 8 percentage-point higher recovery with fibers. Mechanistically, fiber-bridged cracks re-close more effectively, providing preferential pathways for water ingress and stabilizing the microcrack

network; both factors promote re-hydration and secondary precipitation (e.g., C-S-H/carbonates) within defects, thereby restoring stiffness and load transfer.

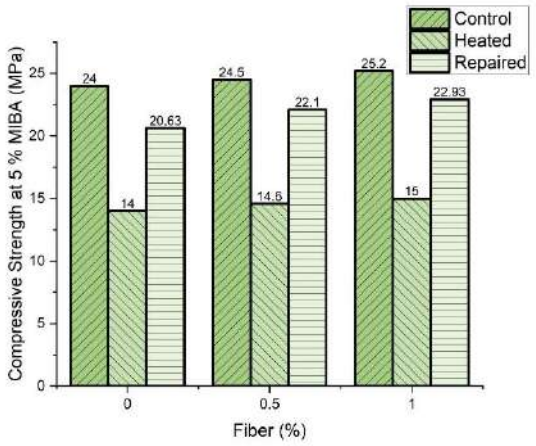
Notably, the relative benefit of fibers is most evident at 10–15% MIBA, where the matrix is intrinsically weaker. The crack-bridging delivers a larger proportional gain in both residual and healed strength. Taken together, these results indicate that while MIBA chiefly governs the baseline matrix quality (with a marked penalty at 15%), steel fibers govern the post-damage pathway, mitigating thermal loss and amplifying strength regain under water curing.



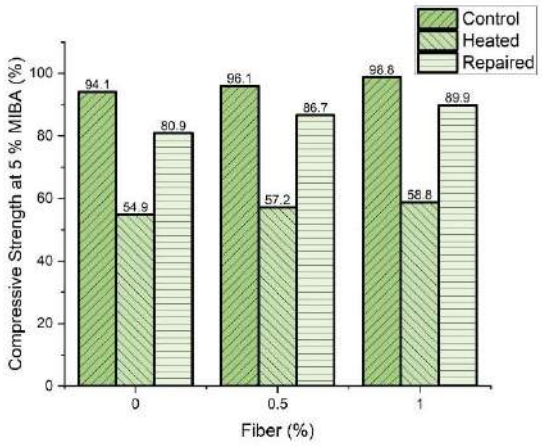

(a)




(b)




(c)




(d)

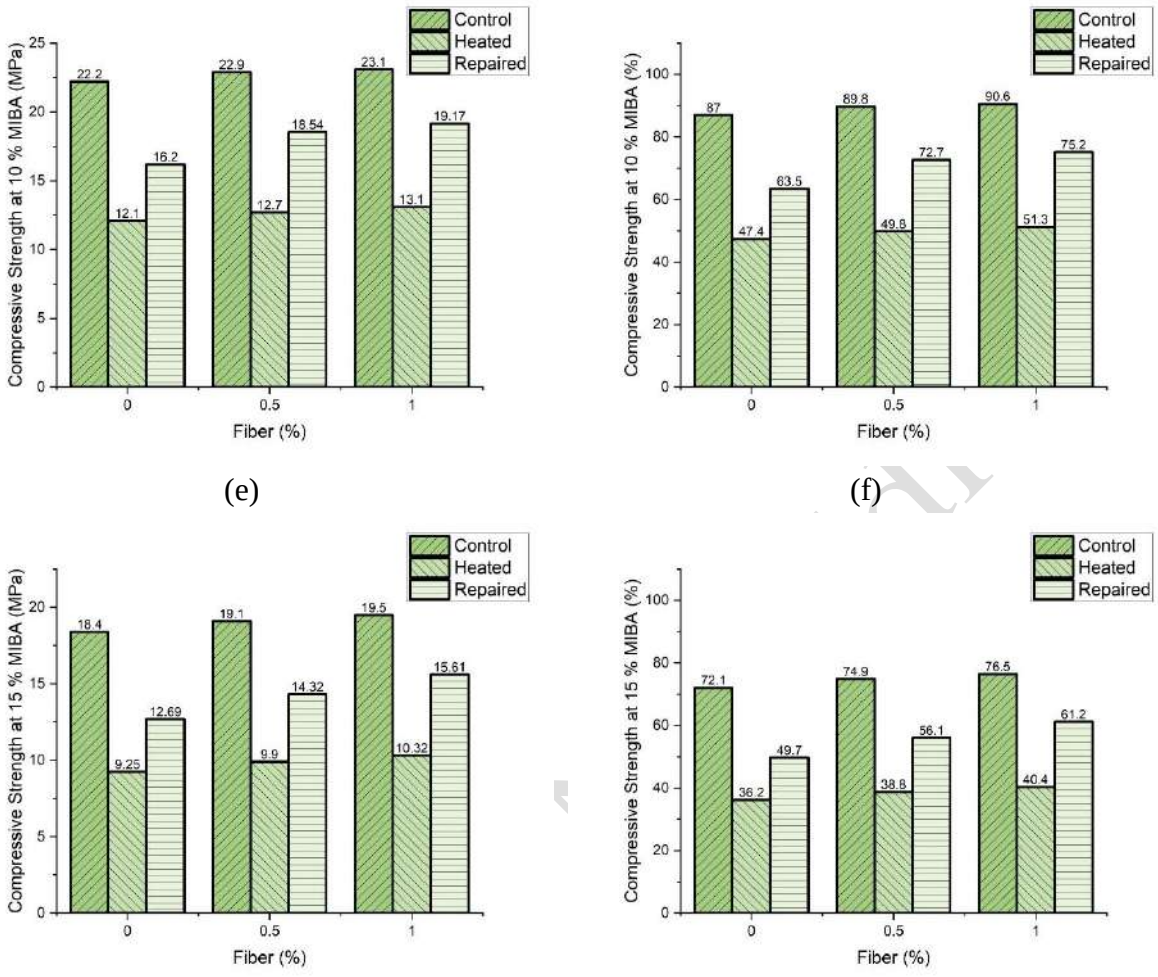



*Figure 6: Effects of Steel Fibers variation on Compressive Strength*

### 3.3 UPV results

Direct-path ultrasonic pulse velocity (UPV) across the 100 mm cube length showed a pronounced loss after heating and a substantial rebound after the 28-day water re-curing. Averaged over all mixes, the baseline velocity before heating was 3.74 km·s⁻¹ (range 3.41–4.12 km·s⁻¹). Exposure to 400 °C reduced the mean to 1.88 km·s⁻¹ (range 1.38–2.31 km·s⁻¹), corresponding to a retained ratio $\frac{V_{heated}}{V_{control}}$ of 0.50 and a damage index $DI = 1 - \frac{V_{heated}}{V_{control}}$ = 0.50. Following water re-curing, the mean velocity increased to 3.16 km·s⁻¹ (range 2.95–3.31 km·s⁻¹), giving a recovery ratio $\frac{V_{repaired}}{V_{control}}$ of 0.85. Expressed as a healing index $DI = 1 - \frac{V_{repaired} - V_{heated}}{V_{control} - V_{heated}}$ the average value was = 0.69, indicating that roughly 70 % of the velocity lost on heating was restored (see Figure 7 and Table 4).

The influence of municipal solid-waste incineration bottom ash (MIBA) on UPV was modest at room temperature and after healing, and more evident in the heated state. Mean baseline velocities

were 3.65, 3.97, 3.81, and 3.55 km·s⁻¹ at 0, 5, 10, and 15 % MIBA, respectively. After heating, the retained ratios $\frac{V_{heated}}{V_{control}}$ increased from 0.44 (0 %) to 0.50 (5 %) and 0.54 (10–15 %), suggesting slightly higher residual continuity at intermediate/upper MIBA levels despite the known strength penalty at 15 %. After re-curing, recovery ratios clustered tightly (0.82–0.90) across all MIBA levels. The corresponding healing indices spanned 0.61–0.78, with the highest mean value at 15 % MIBA. This behavior is consistent with the notion that UPV is primarily sensitive to crack closure and connectivity: mixes with higher capillary porosity can admit water more readily, promoting re-hydration and mineral infill that raise wave speed, even when absolute compressive strength remains comparatively lower.

Steel fibers had little effect on baseline UPV (changes within 0.22 km·s⁻¹ across dosages), but they measurably improved both residual and recovered velocities. The mean retained ratio $\frac{V_{heated}}{V_{control}}$ increased from 0.46 (no fibers) to 0.53 at 0.5–1.0 % fibers. After healing, $\frac{V_{repaired}}{V_{control}}$ rose from 0.80 (no fibers) to 0.86 (0.5 %) and 0.88 (1.0 %). The average healing index increased accordingly (0.63 (at 0 %), 0.69 (at 0.5 %), and 0.75 (at 1.0 % fibers). Mechanistically, fiber bridging constrains thermally induced microcrack widths and maintains path continuity, which both limits the initial drop in wave speed and facilitates moisture ingress and reaction-product precipitation during re-curing.

Overall, UPV decreased by about 50 % after the 400 °C exposure and recovered to about 85 % of the original value after water re-curing. The patterns align with the compressive-strength results: heating degrades stiffness/continuity, while subsequent re-hydration and crack infill restore a large fraction of the transport and load-path connectivity. Notably, UPV tends to rebound more strongly than compressive strength because it is governed by microcrack closure and matrix continuity rather than peak load-carrying capacity. In practical terms, keeping MIBA at or below 10 % limits baseline penalties, and incorporating 0.5–1.0 % steel fibers enhances both residual and recovered UPV, reinforcing the case for pairing fibers with water-activated inorganic healing to improve post-fire performance (Figure 7 and Table 4).

*Table 4: Ultrasonic Pulse Velocity Results*

| MIBA (%) | Fiber (%) | Control µs | Heated µs | Repaired µs |
|---|---|---|---|---|
| 0 | 0 | 24.3 | 71.4 | 32.7 |
| 0 | 0.5 | 29.3 | 72.7 | 32.7 |
| 0 | 1 | 29.2 | 49.2 | 32.2 |
| 5 | 0 | 25.2 | 45.6 | 31.2 |
| 5 | 0.5 | 25.2 | 47.6 | 30.2 |
| 5 | 1 | 25.2 | 59.4 | 30.7 |
| 10 | 0 | 26.7 | 62.9 | 33.9 |
| 10 | 0.5 | 25 | 43.2 | 31.4 |

Accepted / Not Edited

| | | | | |
|---|---|---|---|---|
| 10 | 1 | 27.2 | 43.4 | 30.5 |
| 15 | 0 | 27.7 | 52.4 | 31.7 |
| 15 | 0.5 | 28.2 | 48.1 | 31.2 |
| 15 | 1 | 28.7 | 61.2 | 31.4 |

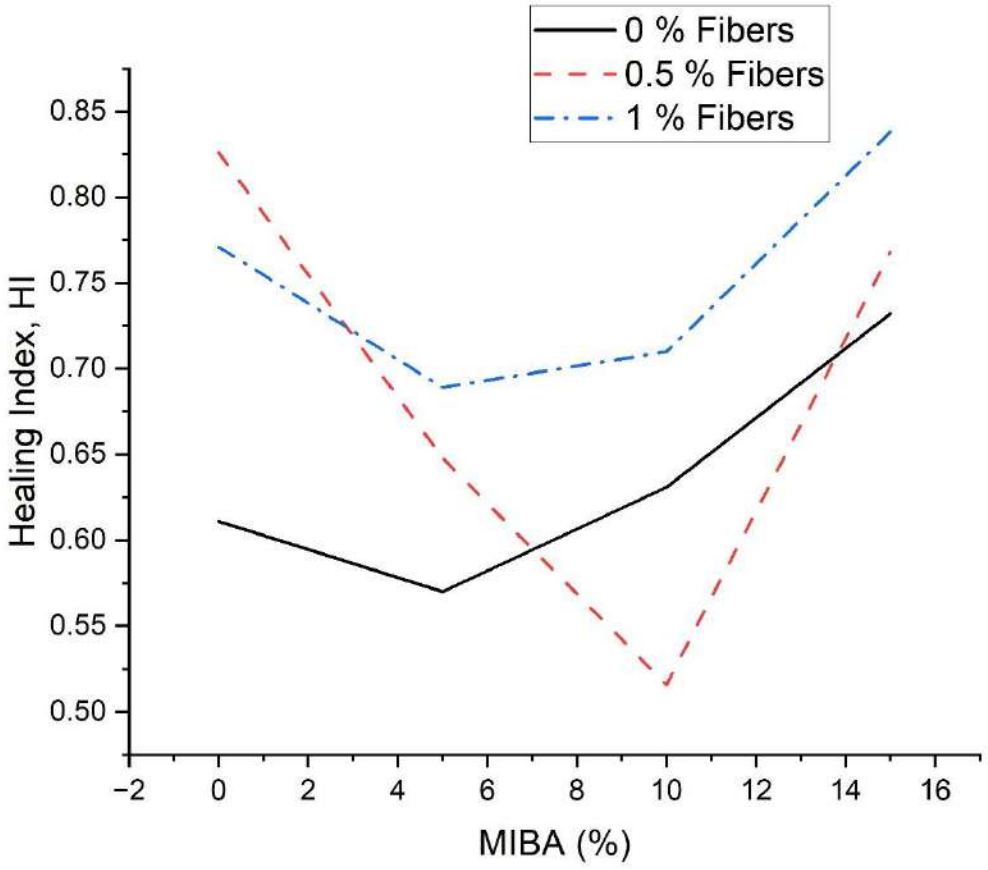



*Figure 7: Healing index vs concentration of MIBA*

## 3.4 Factor effects and interactions (MIBA%, fiber%)

The summary of the absolute and percentage change due to MIBA (0-15%) and steel fibers (0-1.0%) in each conditioning state is summarized in Table 5. Again, MIBA has a much greater effect on baseline strength variation (-7.2 MPa across the range, about 1 MPa for fibers at any fixed MIBA level) and a greater contribution to the post-heating and healed response. The interaction term is small at low MIBA (<0.02) but increases to 0.05 at 15% MIBA, suggesting that the fiber benefit is greater in weaker matrices.

*Table 5: Absolute and relative effects of MIBA and steel fibers across conditioning states*

| Factor | State | Absolute Effect | Relative Effect (%) * |
|---|---|---|---|
| MIBA (0 → 15%) | Control | −7.2 MPa | −27.5 |
| MIBA (0 → 15%) | 400 °C | −0.09 (ratio) | −14.8 |

| | | | |
|---|---|---|---|
| MIBA (0 → 15%) | Healed | −0.19 (ratio) | −20.2 |
| Fiber (0 → 1.0%) | Control | ≤ ±1 MPa | ≤ ±4 |
| Fiber (0 → 1.0%) | 400 °C | +0.021 (ratio) | +3.8 |
| Fiber (0 → 1.0%) | Healed | +0.082 (ratio) | +10.3 |

* Relative to the 0% MIBA / 0% fiber reference in each state.

A two-factor view (MIBA replacement; steel-fiber dosage) clarifies that the baseline matrix quality is governed primarily by the ash content, while fibers matter chiefly once thermal damage and healing are involved. The experimental layout provides sufficient contrast to interpret main effects and their interaction on strength.

Increasing MIBA from 0 to 15 % produces a monotonic decline in compressive strength from 26.2 MPa to 19.0 MPa which is an absolute loss of 7.2 MPa, i.e., 27 % over the range. This shows MIBA as the dominant factor for ambient strength in this study. In practical terms, the penalty is modest up to 10 % but becomes pronounced at 15 %, where both residual capacity and subsequent healing are also depressed, consistent with clinker dilution and higher porosity at elevated replacement levels.

After 400 °C, the retained-strength ratio (Heated/Control) drops with MIBA from 0.61 (0 %) to 0.52 (15 %), an absolute decrease of 0.09 (15 % relative to the 0 % level). Following water curing, the Healed/Control ratio similarly declines from 0.94 (0 %) to 0.75 (15 %), a 0.19 absolute loss (20 % relative). These effect sizes confirm that the ash level continues to influence performance under and after thermal distress, though the penalty is again concentrated at the upper replacement.

At ambient conditions, fibers have little influence on peak compressive strength (changes within ±1 MPa at a given MIBA level), so they are not a significant driver of the control strength in this matrix. Their role becomes consequential after heating and during healing: the 400 °C/Control ratio increases from 0.557 at 0 % fibers to 0.570 (0.5 %) and 0.578 (1.0 %), i.e., +0.013 to +0.021 in absolute terms. Under water curing, the Healed/Control ratio rises from 0.795 (0 %) to 0.855 (0.5 %) and 0.877 (1.0 %), a +0.060 to +0.082 gain. These increments, while small at ambient, are practically meaningful in the post-fire context and align with the expected crack-bridging and microcrack stabilization provided by fibers.

The fiber benefit is most evident at higher MIBA contents (10–15 %), where the matrix is weaker; here, bridging yields a larger proportional improvement in both residual and healed strength. Conversely, at low MIBA, the baseline matrix quality is high enough that fibers contribute mainly to damage tolerance rather than the peak load. This pattern indicates a clear interaction: MIBA controls the starting point (baseline capacity), and fibers improve the trajectory after damage and during recovery.

# 4 Limitations

The present analysis relies on effect-size summaries from three replicates per cell; larger-replication inferential studies are recommended to further validate the interaction trends reported here. Moreover, the study present study focuses on macro-mechanical and non-destructive

Accepted / Not Edited

indicators of post-fire damage and recovery. The mechanistic interpretations offered, including rehydration, C–S–H formation, carbonate precipitation, and fiber–granule synergy, are drawn from the established literature and are not directly verified here by microstructural characterization. A follow-up program incorporating SEM, TGA, and post-healing XRD on the same set of mixes is planned to provide direct experimental confirmation of these mechanisms. The possibility of optimizing dosage and granule size, and comparing it to smaller carrier particles and microencapsulated formulation is seen as a useful avenue for further research.

# 5 Conclusions

This research experimentally investigated the effects of municipal solid waste incineration bottom ash (MIBA), steel fibers, and an inorganic self-healing granulate on concrete subjected to elevated temperature of 400 °C and subsequently re-curing. The main findings are:

1. Increasing MIBA chiefly degrades baseline matrix quality. Compressive strength decreased with replacement level given the performance penalty is modest up to 10% MIBA but becomes pronounced at 15%.
2. Thermal damage reduced capacity for all mixes; residual strength ratios (Heated/Control) declined with MIBA content (0.61 at 0% MIBA to 0.52 at 15%).
3. Water re-curing enabled substantial recovery; healed strength ratios (Healed/Control) were highest at low MIBA (0.94 at 0%) and fell at higher MIBA (0.75 at 15%).
4. Steel fibers had limited effect on peak compressive strength at ambient conditions but improved post-damage behavior, raising residual ratios by 2–4 percentage points and healed ratios by 6–8 points, with the largest proportional gains at higher MIBA. The largest proportional healing gains observed at 10–15% MIBA where fiber bridging constrained crack widths and facilitated moisture-activated self-healing
5. For non-destructive UPV, velocity dropped markedly after heating (47%) and recovered with water re-curing, evidencing moisture-driven crack closing and stiffness restoration. The synergy between fibers (crack-width control) and the inorganic granulate (moisture-activated reactions) underpins the observed recovery.


# Funding

The authors received no financial support or funding for this research.


# Declaration of Generative AI and AI-Assisted Technologies

During the preparation of this manuscript, the authors used AI-assisted tools solely for English language improvement and sentence structuring. The authors take full responsibility for the content, accuracy, interpretation, and conclusions presented in the manuscript.

Accepted / Not Edited

# References


ACI-544.4. (2018). *ACI PRC-544.4-18: Guide to Design with Fiber-Reinforced Concrete*. ACI Farmington Hills, MI.

Arickx, S., Van Gerven, T., & Vandecasteele, C. (2006). Accelerated carbonation for treatment of MSWI bottom ash. *Journal of Hazardous Materials*, *137*(1), 235–243. https://doi.org/https://doi.org/10.1016/j.jhazmat.2006.01.059

ASTM-C138. (2023). *Standard Test Method for Density (Unit Weight), Yield, and Air Content (Gravimetric) of Concrete*. ASTM International.

ASTM-C143. (2015). *Standard Test Method for Slump of Hydraulic-Cement Concrete*. ASTM International.

ASTM-C33/C33M-18. (2018). *Standard Specification for Concrete Aggregates*. ASTM International. https://doi.org/10.1520/C0033_C0033M-18

Astrup, T. (2007). Pretreatment and utilization of waste incineration bottom ashes: Danish experiences. *Waste Management*, *27*(10), 1452–1457. https://doi.org/10.1016/j.wasman.2007.03.017

Bawab, J., Khatib, J., Kenai, S., & Sonebi, M. (2021). A Review on Cementitious Materials Including Municipal Solid Waste Incineration Bottom Ash (MSWI-BA) as Aggregates. In *Buildings* (Vol. 11, Issue 5). https://doi.org/10.3390/buildings11050179

Chang, Y.-F., Chen, Y.-H., Sheu, M.-S., & Yao, G. C. (2006). Residual stress–strain relationship for concrete after exposure to high temperatures. *Cement and Concrete Research*, *36*(10), 1999–2005.

Chen, B., Perumal, P., Illikainen, M., & Ye, G. (2023). A review on the utilization of municipal solid waste incineration (MSWI) bottom ash as a mineral resource for construction materials. *Journal of Building Engineering*, *71*, 106386. https://doi.org/10.1016/j.jobe.2023.106386

De Belie, N., Gruyaert, E., Al-Tabbaa, A., Antonaci, P., Baera, C., Bajare, D., Darquennes, A., Davies, R., Ferrara, L., & Jefferson, T. (2018). A review of self-healing concrete for damage management of structures. *Advanced Materials Interfaces*, *5*(17), 1800074.

Huang, H., Ye, G., & Damidot, D. (2014). Effect of blast furnace slag on self-healing of microcracks in cementitious materials. *Cement and Concrete Research*, *60*, 68–82. https://doi.org/10.1016/j.cemconres.2014.03.010

Lau, A., & Anson, M. (2006). Effect of high temperatures on high performance steel fibre reinforced concrete. *Cement and Concrete Research*, *36*, 1698–1707. https://doi.org/10.1016/j.cemconres.2006.03.024

Li, L., Shi, L., Wang, Q., Liu, Y., Dong, J., Zhang, H., & Zhang, G. (2020). A review on the recovery of fire-damaged concrete with post-fire-curing. *Construction and Building Materials*, *237*, 117564. https://doi.org/10.1016/j.conbuildmat.2019.117564

Lu, Y., Tian, A., Zhang, J., Tang, Y., Shi, P., Tang, Q., & Huang, Y. (2020). Physical and chemical properties, pretreatment, and recycling of municipal solid waste incineration fly ash and bottom ash for highway engineering: A literature review. *Advances in Civil Engineering*, *2020*(1), 8886134.

Ma, Q., Guo, R., Zhao, Z., Lin, Z., & He, K. (2015). Mechanical properties of concrete at high temperature — A review. *Construction and Building Materials*, *93*, 371–383. https://doi.org/10.1016/j.conbuildmat.2015.05.131

Mafalda Matos, A., & Sousa-Coutinho, J. (2022). Municipal solid waste incineration bottom ash recycling


Accepted / Not Edited

in concrete: Preliminary approach with Oporto wastes. *Construction and Building Materials*, *323*, 126548. https://doi.org/10.1016/j.conbuildmat.2022.126548

Magnuson, J. K., Weiksnar, K. D., Patel, A. D., Clavier, K. A., Ferraro, C. C., & Townsend, T. G. (2023). Processing municipal solid waste incineration bottom ash for integration into cement product manufacture. *Resources, Conservation and Recycling*, *198*, 107139. https://doi.org/https://doi.org/10.1016/j.resconrec.2023.107139

Massoumi Nejad, B., Enferadi, S., & Andrew, R. (2025). A comprehensive analysis of process-related CO2 emissions from Iran's cement industry. *Cleaner Environmental Systems*, *16*, 100251. https://doi.org/https://doi.org/10.1016/j.cesys.2024.100251

Modarres, yaghout, & Ghalehnovi, M. (2024). Comparison of the Mechanical Performance of Concrete Reinforced with Recycled Steel Fibers from Waste Tires and Hooked-End Steel Fibers at Ambient and High Temperatures. *Civil Engineering Infrastructures Journal*, *57*(1), 61–83. https://doi.org/10.22059/ceij.2023.349788.1877

Nawaz, M. M., Khan, H. A., Ahmad, J., & Noman, M. (2025). Mechanical performance and life cycle assessment of alkali-activated concrete with municipal-waste incinerated bottom ash as partial precursor. *Multiscale and Multidisciplinary Modeling, Experiments and Design*, *8*(6), 279. https://doi.org/10.1007/s41939-025-00865-5

Noman, M., Khattak, A., Alam, Z., Yaqub, M., & Farsangi, E. N. (2024). Predicting the Residual Compressive Strength of Concrete Exposed to Elevated Temperatures Using Interpretable Machine Learning. *Practice Periodical on Structural Design and Construction*, *29*(4), 4024055. https://doi.org/10.1061/PPSCFX.SCENG-1536

Noman, M., Yaqub, M., Abid, M., Musarat, M. A., Vatin, N. I., & Usman, M. (2022). *Effects of Low-Cost Repair Techniques on Restoration of Mechanical Properties of Fire-Damaged Concrete*. *8*(January), 1–14. https://doi.org/10.3389/fmats.2021.801464

Noman, M., Yaqub, M., Fahad, M., Butt, F., & Khalid, B. (2022). Dynamic Characteristics of RC Structures in Short and Long Duration Real Fires. *Case Studies in Construction Materials*, *16*(February), e01058. https://doi.org/10.1016/j.cscm.2022.e01058

Qian, S. Z., Zhou, J., & Schlangen, E. (2010). Influence of curing condition and precracking time on the self-healing behavior of Engineered Cementitious Composites. *Cement and Concrete Composites*, *32*(9), 686–693. https://doi.org/10.1016/j.cemconcomp.2010.07.015

Silva, R. V, de Brito, J., Lynn, C. J., & Dhir, R. K. (2019). Environmental impacts of the use of bottom ashes from municipal solid waste incineration: A review. *Resources, Conservation and Recycling*, *140*, 23–35. https://doi.org/10.1016/j.resconrec.2018.09.011

Tufail, M., Shahzada, K., Gencturk, B., & Wei, J. (2016). Effect of Elevated Temperature on Mechanical Properties of Limestone, Quartzite and Granite Concrete. *International Journal of Concrete Structures and Materials*, *10*(1), 1–6. https://doi.org/10.1007/s40069-016-0175-2

Van Tittelboom, K., & De Belie, N. (2013). Self-Healing in Cementitious Materials—A Review. In *Materials* (Vol. 6, Issue 6, pp. 2182–2217). https://doi.org/10.3390/ma6062182

Volaity, S. S., Aylas-Paredes, B. K., Han, T., Huang, J., Sridhar, S., Sant, G., Kumar, A., & Neithalath, N. (2025). Towards decarbonization of cement industry: a critical review of electrification technologies for sustainable cement production. *Npj Materials Sustainability*, *3*(1), 23. https://doi.org/10.1038/s44296-025-00068-6

Węgliński, S., & Martysz, G. (2024). Utilization of Municipal Solid Waste Incineration Bottom Ash in

Accepted / Not Edited

Cement-Bound Mixtures. In *Sustainability* (Vol. 16, Issue 5). https://doi.org/10.3390/su16051865

Accepted / Not Edited